Effects of Digital Acquisition Range and Measurement Uncertainty on Stool Footrest Radius Estimates

Wallace, Garrett
Section 25673 Date: 09/14/26

***Abstract*—This measurement examined how digital acquisition range and measurement uncertainty affected the estimates of a stool footrest radius. A strain gauge was bonded to a flexible feeler gauge which measured bending through a quarter Wheatstone bridge. Direct and amplified voltages provided two estimates of curvature while a flexible-tape measurement of the circumference provided an independent comparison. Five sample windows ranging from ±0.64 V to ±10.24 V were examined and all used 2,500 samples per log. The excitation channel saturated in the two smallest windows, 0.64 V & 1.28 V, and the bent-state bridge readings returned zero in the two largest windows. Independent calculations using a flat-state baseline and geometric inputs resulted in radius estimates of approximately 237 ± 36 mm from the direct bridge signal and 237 ± 23 mm from the amplified signal. The measured outside circumference gave a radius of approximately 256.20 ± 0.13 mm with the uncertainty representing an assumed allowance for tape-reading. Both of the electrical uncertainty intervals overlapped in the circumference result under the course uncertainty model. Voltage-difference uncertainty contributed to approximately 63% of the direct-method's variance while sensing-element offset accounted for roughly 82% of the amplified method. A manufacturer drawing provided a supplementary geometric scale check which was used to approximately compare the derived results. The results demonstrated the benefit of amplification for resolving small signals while showing geometric uncertainty, acquisition variation, and incomplete configuration records as limitations of the radius comparison.**

***Index Terms*—Data acquisition, measurement uncertainty, strain gauges, Wheatstone bridges.**

I. Introduction

THE radius of a circular stool footrest can be estimated from its circumference or from the bending strain developed in a flexible metallic strip placed against its surface. These methods provide different measurement paths where measuring the circumference depends on geometric contact and scale while strain measurements depend upon the electrical sensing system and a mechanical model. The laboratory assignment used this comparison to analyze digital data acquisition, voltage resolution, and uncertainty propagation [1]. Digital acquisition represents voltage using discrete levels. Increasing the sample count can improve statistical characterization but does not eliminate saturation, systematic error, or inadequate voltage resolution [2].

A strain gauge is a resistive sensor whose electrical resistance varies when it is deformed. In this experiment, a feeler gauge bonded to another gauge formed the active resistance component in a quarter Wheatstone bridge. This bridge then converted a small resistance change into a measurable voltage, then an amplifier increased said voltage for a second acquisition channel [3]. The strain-dependent voltage was determined relative to its flat state. The strain was then related to and calculated via the curvature using the distance between the strain-sensing element and its neutral axis. This approach assumed that the neutral axis lays at the midpoint of the feeler-gauge thickness and that the gauge followed the curvature of the contacted surface [3]. Root-sum square analysis provided estimates of their total influence and identified which inputs limited each radius estimate [4]. Uncertainties in the gauge factor, voltage, gain, thickness, and sensing-elements led to the uncertainties in the calculated radius.

The objective of this experiment was to examine the effects that five ADC sample windows have on saturation and variability, its relative changes of the estimated footrest radius, and to compare the estimates with outside geometric measurements of the circumference. The analysis also evaluated uncertainty contributions to distinguish the limitations from the electrical and geometric components. A manufacturer drawing supplemented identification and provided a geometric scale check while maintaining the distinction between the published seat dimensions and the experimentally measured diameter.

II. Procedure

A. Apparatus and Specimen Identification

The experiment utilized the laboratory data acquisition system, LabVIEW VI, a quarter Wheatstone bridge with an amplifier assembly, and a strain gauge bonded to a flexible metal feeler gauge. The apparatus followed the arrangement described in the laboratory materials provided [3]. Separate channels on the assembly recorded excitation voltage V_s, amplified voltage V_{amp}, and direct voltage V_g.

The chair label identified the specimen as Steelcase model TS31202B, corresponding to the Shortcut Five-Star Base Stool in the manufacturer's specification guide (Fig. 1) [5].

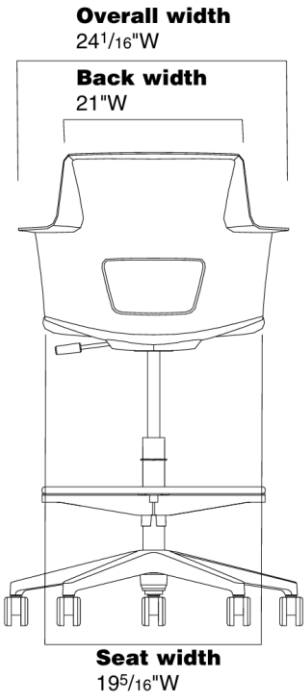


Fig. 1. Manufacturer drawing of the Steelcase Shortcut Five-Star Base Stool. The footrest is slightly larger than the specified seat width, providing a visual scale check. Reproduced from [5, p.366]

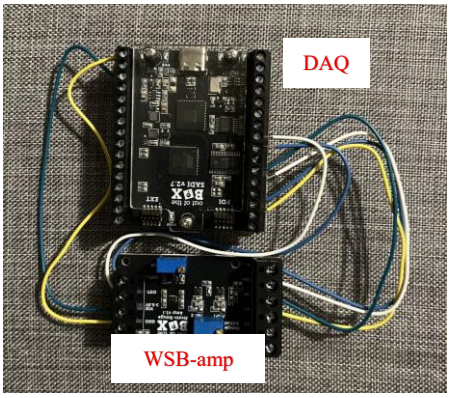


Fig. 2(a). Front of experimental apparatus and electrical measurement paths. The direct and amplified outputs provided separate voltage measurement of the bending.

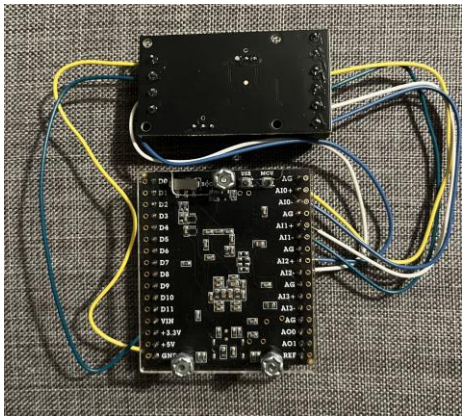


Fig. 2(b). Back of experimental apparatus and electrical measurement paths. The direct and amplified outputs provided separate voltage measurement of the bending.

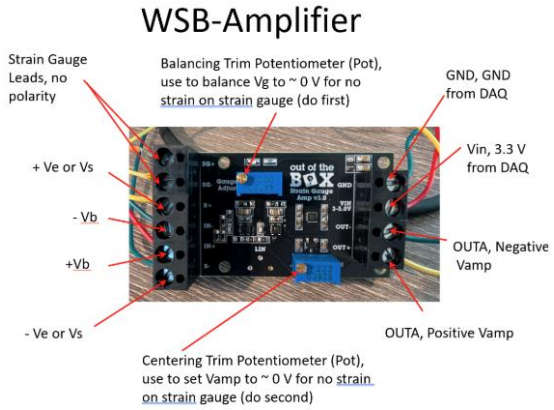


Fig. 3. WSB-amplifier terminal assignments and adjustment controls identifying the inputs, DAQ connections, and outputs. Reproduced from [3].

B. Geometric Inputs and Surface Definition

The feeler-gauge thickness used in the laboratory was t = 0.40 mm, and the distance from the feeler-gauge surface to the center of the sensing element was d=0.03 mm. These inputs gave a neutral-axis-to-sensor distance of 0.230 mm. Their assigned uncertainties followed the laboratory instructions [1].

The gauge factor was taken as $G_f = 2.0$, and the amplifier gain magnitude was labeled as A = 900 by following the supplied laboratory values [1]. The uncertainties assigned to each of these values are listed in the appendix.

The circumference measurement described the outermost surface of the footrest ring. The strain-derived contact radius was interpreted to be the radius of the same outermost surface. This required the feeler gauge to follow that surface with its sensing element on the outermost side of the strip [3].

C. Sample-Window Exploration

Five files represented the sample windows ±0.64, ±1.28, ±2.56, ±5.12, and ±10.24 V. Each file contained six saved data points where the first three had small strain-related values while the final three described the bending response. These groups were classified as flat and bent conditions, respectively.

Each acquisition used 2,500 samples to calculate voltage means and standard deviations. The saved columns contained elapsed time, the three voltage measurements and their standard deviations, two calculated strains, and two calculated radii. This analysis maintained the voltage signs and distinguished the measured values from derived values.

For each window and condition, the three saved voltage means were averaged. The means of the three exported standard deviations summarized the variability of the sample-window tables. This statistic was not considered as the standard deviations of the three saved means. The first part of this analysis reports standard deviations rather than requiring the uncertainty intervals for window-exploration results [1].

For a bipolar ADC window with limits V_{min} and V_{max}, the increment was calculated as

$$q = \frac{(Vmax - Vmin)}{2^n} \qquad (1)$$

where n = 14 was the bit depth used in the analysis. This divided the full span into 2^{14} = 16,384 intervals in the code. The resolution described a voltage increment, not the accuracy of the complete system [2].

D. Dedicated Stool Measurements and Baseline Treatment

The dedicated stool file contained three acquisitions near 23 s and three near 61 s. The earlier group had small strain-related signals and was interpreted as flat; the latter group was interpreted as bent. Channel windows were ±2.56 V for V_s, ±0.64 V for V_g, and ±1.28 V for V_{amp}. Because the original tare-control entries were unavailable, voltage changes were calculated by subtracting the inferred flat-group means from the bent-group means.

The prescribed procedure included measuring the flat condition and entering tare voltages before bending [1]. The exact original tare-control values from the lab were unavailable. This then means that the calculated voltage changes from the recorded groups are:

$$\Delta V_g = V_{g,b} - V_{g,f}, \tag{2}$$

$$\Delta V_a = V_{a,b} - V_{a,f}, \tag{3}$$

Where *f* and *b* denoted inferred flat and bent conditions while *a* denoted amplified channel. This subtraction operated on strictly the voltage measurements, not to the tare correction to the already calculated strain values.

E. Strain and Radius Calculations

The direct and amplified strains were calculated using the provided quarter-bridge relationship [3]:

$$\varepsilon_g = \frac{4|\Delta V_g|}{V_s G_f}, \tag{4}$$

$$\varepsilon_a = \frac{4|\Delta V_a|}{A V_s G_f}. \tag{5}$$

The mean bent-state voltage was utilized in both expressions. From these calculations, the measured amplified change was negative while the direct change was positive. The magnitudes were used for the physical radius calculation while the voltages with varies signs were retained.

The neutral-axis-to-sensor distance was

$$y = d + \frac{t}{2}. \tag{6}$$

The neutral axis radius was ρ = y / ε. The contact radius was found by subtracting half the feeler-gauge thickness [3]:

$$r_i = \frac{d + \frac{t}{2}}{\varepsilon} - \frac{t}{2}. \tag{7}$$

Combining the electrical and geometric equations resulted in the following equations:

$$r_{i,g} = \frac{\left(d + \frac{t}{2}\right) V_s G_f}{4|\Delta V_g|} - \frac{t}{2} \tag{8}$$

$$r_{i,a} = \frac{\left(d + \frac{t}{2}\right) A V_s G_f}{4|\Delta V_a|} - \frac{t}{2} \tag{9}$$

These equations defined methodology behind all calculations utilized in this lab.

F. Circumference Measurement

The measured outermost circumference was approximately 1609.7 mm (63 3/8 in). The unrounded converted value, 1609.725 mm, was retained for calculation. The circumference-derived radius equation was:

$$r_C = \frac{C}{2\pi}. \tag{10}$$

The smallest tape measurement interval was 1/16-in. The laboratory half-division rule then gave a reading allowance of 0.79375 mm [1].



Fig. 4. Strain-gauge and feeler-gauge assembly secured against the outer surface of the stool footrest. Note that the electrical components of the strain gauge are on the outermost surface of the feeler gauge.

III. Results

The results comprised voltage measurements across five sample windows, stool measurements, and radius estimates that were directly obtained from direct bridge voltage, amplified bridge voltage, and the circumference. These window measurements documented changes in the recorded voltage levels and variability (Tables I-III). The measurements provided for the inputs for the independent radius calculations (Tables IV-V) while the uncertainty analysis quantified each inputs contribution to resulting radius variance (Table VI).

A. Excitation Voltage and ADC Resolution

The excitation channel returned means near the positive range limit in the two smallest windows with zero recorded standard deviation. In the other windows, the mean excitation voltage was approximately 2.498-2.499 V (Table I).

TABLE I
Excitation voltage and nominal ADC increment

Window (V)	*q* (mV)	Flat mean V_s (V)	Flat mean *s* (mV)	Bent mean V_s (V)	Bent mean *s* (mV)
± 0.64	0.078125	0.639922	0	0.639922	0
± 1.28	0.15625	1.279844	0	1.279844	0
± 2.56	0.31250	2.499268	0.152	2.499242	0.159
± 5.12	0.62500	2.498411	0.113	2.498414	0.103
± 10.24	1.2500	2.497809	0.0677	2.497806	0.0453

Each condition contained three acquisitions of 2,500 samples. "Mean s" was the arithmetic mean of the exported standard deviations. Additional digits within the voltage means were retained to identify small differences.

B. Direct and Amplified Bridge Measurements

The bent direct-bridge means were nonzero in the three smaller windows. However, in the ±5.12 and ±10.24 V files, the bent means and standard deviations were zero (Table II). This then caused the corresponding saved radius outputs to be registered as infinite.

TABLE II
DIRECT BRIDGE VOLTAGE BY SAMPLE WINDOW

Window (V)	Flat mean V_g (V)	Flat mean *s* (mV)	Bent mean V_g (V)	Bent mean *s* (mV)
± 0.64	-0.0110	0.0343	0.9253	0.0557
± 1.28	-0.0223	0.0543	1.0860	0.0590
± 2.56	-0.0560	0.1193	0.9043	0.0960
± 5.12	-0.8133	0.2870	0	0
± 10.24	-0.3193	0.5443	0	0

Grouping and averaging followed Table I. Zero is a recorded output rather than a physical input

The amplified bent means +0.640000 V with zero standard deviation in the smallest window. The other windows contained negative bent means with magnitudes between approximately 1.065 and 1.144 V (Table III).

TABLE III
AMPLIFIED BRIDGE VOLTAGE BY SAMPLE WINDOW

Window (V)	Flat mean V_{amp} (V)	Flat mean *s* (mV)	Bent mean V_{amp} (V)	Bent mean *s* (mV)
± 0.64	0.000578	7.192	0.640000	0
± 1.28	-0.000797	3.894	-1.143838	6.316
± 2.56	0.000540	3.831	-1.143471	7.982
± 5.12	-0.012643	4.039	-1.065348	8.419
± 10.24	-0.018858	4.059	-1.137463	8.189

Grouping and averaging followed Table I. Signs were preserved.

C. Stool Measurement Averages

The dedicated stool means were 2.499234 V in flat condition and 2.499245 V in bent condition. The bridge mean changed from 0.037 mV to 1.248 mV, while the amplified mean differed from 0.003121 to -1.085513 V.

TABLE IV
STOOL VOLTAGE MEANS AND ADOPTED MEASUREMENT UNCERTAINTIES

Quantity	Flat mean	Bent mean
V_s (V)	2.49923 ± 0.00032	2.49925 ± 0.00032
V_g (mV)	0.037 ± 0.092	1.248 ± 0.11
V_{amp} (V)	0.003 ± 0.013	-1.086 ± 0.022

The means summarize three acquisitions per condition. Uncertainty allowance follows the course's twice-standard-deviation convention, they are not confidence intervals for the averaged means. Unrounded values were later used in calculations.

Equations (2) and (3) gave corrected changes of 1.211 ± 0.15 mV for the direct channel and -1.089 ± 0.025 V for the channels that were amplified. The original mean bent-state VI outputs were 239.80 mm and -252.82 mm. These values are the saved software results, not the independently re-evaluated estimates below.

The directly measured circumference and its assumed allowances were 1609.73 ± 0.79 mm and the resulting circumference radius was 256.20 ± 0.13 mm.

D. Calculated Strain and Radius

The independently calculated radii were 237 ± 36 mm from the direct bridge signal, 237 ± 23 mm from the amplified signal, and 256.20 ± 0.13 mm from circumference (Table V).

TABLE V
INDEPENDENTLY CALCULATED FOOTREST RADII

Method	Radius (mm)	Approximate comparison interval (mm)
Direct bridge	237 ± 36	201 - 273
Amplified bridge	237 ± 23	215 - 260
Circumference	256.20 ± 0.13	256.07 - 256.33

Intervals were calculated prior to rounding. The electrical uncertainties are first-order RSS estimated under the adopted course model. The circumference allowance only includes the uncertainties within the reading.

The unrounded electrical point estimates were 237.135 and 237.411 mm which was a difference of 0.276 mm. Their deviations from the circumference estimations were -7.44% and -7.33% respectively. These percentages were not calibrated accuracy specifications but rather compared point estimates.

E. Uncertainty Contributions

The direct voltage difference contributed roughly 63% of the direct method's variance. The offset *d* contributed roughly 82% for the amplified method (Table VI).

TABLE VI
PERCENTAGE CONTRIBUTIONS TO RADIUS VARIANCE

Input	Direct method (%)	Amplified method (%)
Voltage difference	63.0	5.82
Sensing offset *d*	32.3	82.1
Feeler-gauge thickness *t*	4.54	11.5
Gauge factor G_f	0.107	0.271
Amplifier gain A	Not applicable	0.271
Excitation voltage V_s	<0.001	<0.001

Contributions were calculated from unrounded values. Displayed percentages may not sum to exactly 100%.

IV. Discussion

This experiment evaluated how ADC sample-window selection and uncertainty measurements can affect estimates of a footstool radius. The two smallest windows saturated the excitation channel while the two largest windows produced zero bent-state bridge outputs. The independent calculations from the stool measurements gave radii of approximately 237 ± 36 mm and 237 ± 23 mm from direct and amplified signals, respectively. Both of these uncertainty intervals overlapped the circumference result of 256.20 ± 0.13 mm under the uncertainty model. These findings supported that suitable acquisition ranges and characterization of provided geometric inputs are necessary for result interpretation.

A. Saturation and Appropriate Channel Ranges

The excitation measurements in the ± 0.64 and ± 1.28 V windows demonstrated saturation. Their values stayed near the positive limit despite approximately 2.5 V excitation measurements in the larger windows. The zero recorded standard deviations indicated repeated outputs, not accurate measurements of the voltage [2].

Underestimating excitation voltage increases calculated strain for a fixed bridge-voltage change and therefore decreases the radius calculated from (7). The radii obtained using saturated excitation readings were consequently unreliable.

The amplified bent reading also reached the + 0.64 V limit in the smallest window size. Despite the positive sign differing from other negative readings in the other filed, its zero standard deviation showed to be consistent with clipping. This is primarily caused by ADC range selection but also via differences in bending direction, wiring, adjustment, or acquisition states. The above analysis preserved the sign discrepancy as an experimental observation.

B. Resolution, Standard Deviation, and Zero Outputs

The ADC increment increased by a factor of sixteen between the smallest and largest windows, leading to the small bridge signal occupying fewer digital intervals as the range widened. In the same idea, the largest window showed the 1.25 mV increment was the same order as the stool's 1.211 mV voltage change. This comparison demonstrated why direct measurement was susceptible to the loss of useful amplitude information.

The bent bridge outputs were zero in the ± 5.12 and ± 10.24 V windows, preventing a usable radius calculation. These results were consistent with insufficient resolution for the small bridge signal, although the recorded data did not establish the cause conclusively. A zero digital output did not demonstrate the idea of zero physical strain.

The flat bridge standard deviation increased from approximately 0.034 mV to 0.544 mV as the sample windows grew, however, the excitation-channel variability decreased over some of the larger windows. These observations showed that the ADC resolution and measured standard deviations are distinct and that repeated identical digital readings could produce small amounts of variability without showing an accurate measurement [2].

C. Radius Agreement and Amplifier Consistency

The two independently calculated electrical radii differed by approximately 0.12% of their mean. To support this calculation, a supporting check of the ratio of the baseline voltage changes:

$$A_{effective} = \frac{|\Delta V_a|}{|\Delta V_g|} = 898.95. \quad (11)$$

The effective gain was consistent with the nominal magnitude of 900. Its propagated uncertainty was approximately 1.1 x 10^2, so, this comparison provided a consistency check rather than a precise calibration.

Both electrical point estimates were approximately 19 mm below the circumference estimate and their adopted uncertainty intervals included the circumference result. Utilizing the laboratory interval-comparison approach, the estimates were similar within the modeled uncertainty [1]. This statement was dependent upon the input uncertainties, first order RSS model, and treatment of the voltage variability.

The calculation methods also shared common geometric and electrical inputs. Having a common error within the d, t, or gauge factor could shift both of the electrical estimates into the same direction. Their central values being similar to one another is valuable evidence of consistency, yet the circumference measurement and contact geometry remained as helpful external checks.

D. Manufacturer Drawing and Geometric Comparison

The manufacturer specified a seat width of approximately 490.5 mm (19 5/16 in), and the footrest slightly extended past the corresponding dimension lines (Fig 1.) [5, p. 366]. The measured circumference gave an outside footrest diameter of 512.39 ± 0.25 mm, approximately 4.5% greater than the specified seat width. This relationship appeared to be visually consistent with the manufacturer drawing and supported the plausibility of the circumference measurement. Despite this, the seat width was not a specified diameter, so the comparison it a scale check rather than an accuracy approval.

E. Saved VI Outputs and Independent Calculations

The independently recalculated radii differed from the original VI outputs. The saved amplified-radius magnitude averaged at 252.82 mm while the independent gave approximately 237.41 mm. The values used the inferred flat-group average, laboratory-specified gain, laboratory-specified gauge factor, and geometry. Due to the original tare entries being unavailable, the certain cause of the discrepancy could not be established. Due to this, the saved outputs were retained separately from the results.

F. Dominant Uncertainty and Improvements

The voltage-difference uncertainty contributed to approximately 63% of the direct method's propagated variance. If there were improved connection stability, controlled baseline acquisition, and reduced electrical interference, there would have been visible improvements. The direct channel utilizes the smallest tested sample window, thus, further gain values would require improved signal conditioning or greater hardware resolution.

For the amplified method, voltage uncertainty contributed to approximately 5.8% of the propagated variance while the uncertainty in the sensing element, d, contributed approximately 82%. The assigned offset uncertainty of 0.020 mm was relatively large compared to its value of 0.030 mm. Verifying the sensing-element position and feeler gauge thickness would have therefore offered greater improvements than a reduction in the amplifier noise [1], [3].

The bent amplifier means had a standard deviation of approximately 0.0192 V between acquisitions, which exceeded the representative value of approximately 0.0109 V within acquisitions. This demonstrated that the within-acquisition uncertainty model did not effectively capture all variation between the values saved. By introducing repeated placement trials where each had a fresh baseline, there would distinguishably help in the electrical variability from changes within contact or positioning.

The circumference uncertainty only included an assumed reading allowance. Tension within the tape, stretch, alignment, and measurement-path variation effects were not effectively quantified, thus, the reported radius uncertainty of 0.13 mm did not establish accuracy at that level. Repeating the circumference measurement multiple times would have strengthened the comparison.

Future exports regarding this lab should preserve state labels, channel ranges, sample counts, gain, gauge factor, tare values, and geometric inputs for proper re-experimentation. These records would then allow for the original calculations to be reproduced and reduce the reliance upon settings.

These conclusions apply to the tested stool, sensing assembly, and the recorded measurement conditions. The quantitative radius estimate is dependent upon the geometric and acquisition setting, a flat-state baseline, and a tape graduation measurement. The uncertainty model also excluded unquantified placement effects, tape-path errors, and drift during measurements, so, internal overlap did not justify the absence of systematic bias. The need to avoid saturation and resolve small bridge signals applies to similar strain measuring systems, however, the numerical radius and uncertainty contributions cannot be generalized to other systems or configurations without additional measurements.

V. Conclusion

The experiment demonstrated that acquisition-range selection impacted both the voltage measurements and strain-derived geometry. The two smallest sample windows saturated within the excitation channel while the two largest windows produced unusable bent-state bridge outputs of zero. Independent processing of the stool data gave radius estimates of approximately 237 ± 36 mm and 237 ± 23 mm from the direct and amplified channels, respectively. Both of the adopted uncertainty intervals overlapped the derived circumference result of 256.20 ± 0.13 mm. The measured footrest diameter was approximately 4.5% greater than the manufacturers specified seat width, which was consistent with the drawing's appearance and proved to be useful as a geometric scale check. The drawing did not specify the footrest diameter, thus the drawing could not be used as an accuracy comparison. Uncertainty within voltage-difference dominated the direct method while uncertainty within the sensing element offset dominated the amplified method. Verification of the geometry and repeated placement of baseline measurements along with the preservation of acquisition settings would prove to be the most useful improvements.

Appendix: Uncertainty Analysis

A. Given and Assumed Inputs

The feeler-gauge thickness and sensing offset used in the laboratory were t = 0.400 mm and d = 0.030 mm. These uncertainties, coupled with the gauge factor and amplifier gain, followed the provided assignment's uncertainty table [1]. The circumference-reading allowance followed the half-division rule using a tape graduation of 1/16 in. These inputs and their uncertainty sources are listed in Table VII.

TABLE VII
Given and Assumed Input Uncertainties

Input	Uncertainty symbol	Absolute uncertainty	Source
Feeler gauge thickness t	U_t	0.015 mm	Laboratory input; specified in [1]
Sensing offset d	U_d	0.020 mm	Laboratory input; specified in [1]
Gauge factor G_f	U_{Gf}	0.010	Manufacturer value and uncertainty supplied in [1]
Amplifier gain magnitude A	U_A	4.5	Manufacturer value and uncertainty supplied in [1]
Outside circum. C	U_C	0.79 mm	Measurement; graduation and half-division rule [1]
Math constant π	-	Negligible numerical grant	Python

The gauge-factor and amplifier-gain uncertainties were specified as 0.50% of their respective values [1]. Their absolute uncertainties were

$$U_{G_f} = 0.005G_f = 0.010, U_A = 0.005A = 4.5. \quad (12)$$

The tape graduation is used as a 1/16-in division, consistent with comparable flexible tape. Applying the laboratory half-division rule gave

$$U_C = \frac{1}{2}\left(\frac{1}{16}in\right)\left(25.4\frac{mm}{in}\right) = 0.79375\ mm. \quad (13)$$

This value was reported at 0.79 mm. The assignments typical 0.5-mm tape allowance was not treated as a specification for the instrument used. The adopted allowance represented uncertainty within the reading and excluded unquantified effects from elements like tension, alignment, stretch, and path.

The mathematical constant π had no physical measurement uncertainty. Its numerical approximation contributed negligibly when regarding the reported precision.

B. Statistical Voltage Uncertainties

Each saved acquisition contained 2,500 samples. Three of these acquisitions represented each flat and bent condition. For each voltage channel and condition, the exported standard deviations s_1, s_2, and s_3, were combined using

$$s_{rep} = \sqrt{\frac{s_1^2 + s_2^2 + s_3^2}{3}}, \tag{14}$$

where s_{rep} was the representative within-acquisition standard deviation. This calculation combined the variances within acquisition without including the variation between the acquisition means.

The course's large-sample uncertainty convention was then applied [2], [4]:

$$U_V = 2s_{rep}, \tag{15}$$

where U_v was the adopted voltage measurement uncertainty allowance. The resulting values are then listed in Table VIII.

TABLE VIII
STATISTICAL VOLTAGE UNCERTAINTY ALLOWANCES

Quantity	Uncertainty symbol	Samples per acquisition	Trials	Uncertainty (V)
Flat excitation voltage	$U_{Vs,f}$	2,500	3	0.00032
Bent excitation voltage	$U_{Vs,b}$	2,500	3	0.00032
Flat direct bridge voltage	$U_{Vg,f}$	2,500	3	0.000092
Bent direct bridge voltage	$U_{Vg,b}$	2,500	3	0.00011
Flat amplified voltage	$U_{Va,f}$	2,500	3	0.013
Bent amplified voltage	$U_{Va,b}$	2,500	3	0.022

Subscripts f and b denote inferred flat and bent conditions while a denotes the amplified channel. Uncertainties were developed statistically using (14) and (15), not from manufacturer specifications.

The twice-standard deviation approximated 95% of the measurement coverage under the course assumptions of a sufficiently large Gaussian sample set [2], [4]. These allowances were not divided by the square root of the sample count and thus were not interpreted as formal confidence intervals for the group means. Unrounded statistical values were kept through the propagation calculations and the displayed uncertainties were rounded to two significant figures.

C. RSS Propagation of Voltage Differences

For a reliable differential result z determined by independent uncertain inputs x_j, first order RSS propagation was used [4]

$$U_z^2 = \Sigma \left(\frac{\delta z}{\delta x_j} U_{x_j}\right)^2, \tag{16}$$

where U_z was the propagated uncertainty value and U_{xj} was the uncertainty assigned to the input, x_j.

Applying (16) to the direct voltage difference in (2) gave

$$U_{\Delta V_g}^2 = \left(\frac{\delta \Delta V_g}{\delta V_{g,b}} U_{V_{g,b}}\right)^2 + \left(\frac{\delta \Delta V_g}{\delta V_{g,f}} U_{V_{g,f}}\right)^2. \tag{17}$$

For the amplified voltage difference in (3),

$$U_{\Delta V_a}^2 = \left(\frac{\delta \Delta V_a}{\delta V_{a,b}} U_{V_{a,b}}\right)^2 + \left(\frac{\delta \Delta V_a}{\delta V_{a,f}} U_{V_{a,f}}\right)^2. \tag{18}$$

These expressions assumed independent flat and bent measurement errors. The resulting uncertainties were 0.1470 mV for the direct difference and 0.02521 V for the amplified difference prior to rounding. Thus, the reporting uncertainty magnitudes were therefore 0.15 mV and 0.025 V. The sensitivity coefficients for subtraction were +1 and −1, so both squared uncertainty terms contributed positively to the combined variance [4].

D. RSS Propagation of Strain

Applying RSS to the direct strain relationship in (4) gave

$$U_{\varepsilon_g}^2 = \left(\frac{\delta \varepsilon_g}{\delta \Delta V_g} U_{\Delta V_g}\right)^2 + \left(\frac{\delta \varepsilon_g}{\delta V_s} U_{V_s}\right)^2 + \left(\frac{\delta \varepsilon_g}{\delta G_f} U_{G_f}\right)^2. \tag{19}$$

For the amplified strain relationship in (5),

$$U_{\varepsilon_a}^2 = \left(\frac{\delta \varepsilon_a}{\delta \Delta V_a} U_{\Delta V_a}\right)^2 + \left(\frac{\delta \varepsilon_a}{\delta V_s} U_{V_s}\right)^2 + \left(\frac{\delta \varepsilon_a}{\delta G_f} U_{G_f}\right)^2 + \left(\frac{\delta \varepsilon_a}{\delta A} U_A\right)^2. \tag{20}$$

The excitation uncertainty was taken from the bent condition due to its mean excitation voltage being used in the strain calculations. The propagated strain uncertainties were 0.00012 mm/mm for the direct method and 0.000023 mm/mm for the amplified method. These calculations used the magnitudes of the base corrected voltage changes. The amplified-strain calculation also included the component of gain uncertainty [4].

E. RSS Propagation of Contact Radius

The contact-radius uncertainties were propagated through the combined electrical and geometric expressions in (8) and (9). This demonstrated the dependence upon thickness in both the sensing element distance and the contact-radius correction. Treating these two appearances of t as independent would have been misrepresentation. A single derivative with respect to thickness therefore accounted for its combined effect on both parts of the radius equation [4]

For the direct method,

$$U_{r_{i,g}}^2 = \left(\frac{\delta r_{i,g}}{\delta t} U_t\right)^2 + \left(\frac{\delta r_{i,g}}{\delta d} U_d\right)^2 + \left(\frac{\delta r_{i,g}}{\delta V_s} U_{V_s}\right)^2 + \left(\frac{\delta r_{i,g}}{\delta G_f} U_{G_f}\right)^2 + \left(\frac{\delta r_{i,g}}{\delta \Delta V_g} U_{\Delta V_g}\right)^2. \quad (21)$$

For the amplified method,

$$U_{r_{i,a}}^2 = \left(\frac{\delta r_{i,a}}{\delta t} U_t\right)^2 + \left(\frac{\delta r_{i,a}}{\delta d} U_d\right)^2 + \left(\frac{\delta r_{i,a}}{\delta V_s} U_{V_s}\right)^2 + \left(\frac{\delta r_{i,a}}{\delta G_f} U_{G_f}\right)^2 + \left(\frac{\delta r_{i,a}}{\delta A} U_A\right)^2 + \left(\frac{\delta r_{i,a}}{\delta \Delta V_a} U_{\Delta V_a}\right)^2. \quad (22)$$

The unrounded propagation uncertainties were 36.294 mm for the direct method and 22.802 mm for the amplified method. Rounding these values to two significant figures provides the reported radius estimates of 237 ± 36 mm and 237 ± 23 mm, respectively. These allowances followed the adopted first-order RSS model and did not include the quantified contribution from drift, gauge placement, or uncertainty within the original tare-controlled entries.

F. RSS Propagation of Circumference Radius & Diameter

Applying RSS to the circumference relationship in (10) gives

$$U_{rC}^2 = \left(\frac{\delta rC}{\delta C} U_C\right)^2. \quad (23)$$

The propagated uncertainty was 0.12633 mm prior to rounding, resulting in a reported radius of 256.20 ± 0.13 mm.

The outside diameter used in the manufacturer comparison is

$$D_C = \frac{C}{\pi}, \quad (24)$$

where D_C was the circumference-derived outside diameter. The uncertainty equation was

$$U_{D_C}^2 = \left(\frac{\delta D_C}{\delta C} U_C\right)^2. \quad (25)$$

The resulting diameter was 512.39 ± 0.25 mm. Both of the circumference uncertainty allowances only included the assumed reading contribution without consideration for the manufacturing tolerances or dimensions. Because diameter was twice the radius, its absolute uncertainty was also twice the radius uncertainty before rounding.

G. Effective-Gain Uncertainty and Variance Contributions

The effective-gain ration in (11) compared the magnitudes of the amplified and direct voltage changes. With independent channel errors being considered, its uncertainty was

$$U_{A_{effective}}^2 = \left(\frac{\delta A_{effective}}{\delta \Delta V_a} U_{\Delta V_a}\right)^2 + \left(\frac{\delta A_{effective}}{\delta \Delta V_g} U_{\Delta V_g}\right)^2. \quad (26)$$

The propagated uncertainty was approximately 1.1 x 10^2. The correlation between the direct and amplified measurements were not quantifies, thus, the allowance was conditional on the stated independence.

The percentage contribution of input x_j to the total variance of the total radius was calculated as

$$P_j = 100 \frac{\left(\frac{\delta r}{\delta x_j} U_{x_j}\right)^2}{U_r^2}, \quad (27)$$

where P_j was the percentage contribution and U_r^2 was the total radius variance.

TABLE IX
SUMMARY OF PROPAGATED UNCERTAINTIES

Calculated quantity	Uncertainty symbol	Uncertainty magnitude	Method
Direct voltage difference	$U_{\Delta V_g}$	0.15 mV	RSS, (17)
Amplified voltage difference	$U_{\Delta V_a}$	0.025 V	RSS, (18)
Direct strain	U_{ε_g}	0.00012 mm/mm	RSS, (19)
Amplified strain	U_{ε_a}	0.000023 mm/mm	RSS, (20)
Direct contact radius	$U_{r_{i,g}}$	36 mm	RSS, (21)
Amplified contact radius	$U_{r_{i,a}}$	23 mm	RSS, (22)
Circumference radius	U_{r_C}	0.13 mm	RSS, (23)
Circumference diameter	U_{D_C}	0.25 mm	RSS, (25)
Effective gain	$U_{A_{effective}}$	1.1 x 10^2	RSS, (26)

REFERENCES

[1] S. Ridgeway, "Lab 1 assignment," EML 3301C Mechanics of Materials Laboratory, pp. 1-3, Gainesville, FL: University of Florida, 2026, unpublished.

[2] S. Ridgeway, "MOM_lab uncertainty direct measurements," EML 3301C Mechanics of Materials Laboratory, pp. 1-40, Gainesville, FL: University of Florida, 2026, unpublished.

[3] S. Ridgeway, "Lab 1 introduction," EML 3301C Mechanics of Materials Laboratory, pp. 1-15, Gainesville, FL: University of Florida, 2026, unpublished.

[4] S. Ridgeway, "MOM_lab uncertainty propagation," EML 3301C Mechanics of Materials Laboratory, pp. 1-20, Gainesville, FL: University of Florida, 2026, unpublished.

[5] Steelcase, "Shortcut," *Seating Specification Guide*, pp. 366, 369, June 2023. [Online]. Available: Manufacturer specification guide hosted by Designfarm Accessed: Sept. 13, 2026.